# KU LEUVEN

## STADIUS
Center for Dynamical Systems,
Signal Processing and Data Analytics

*(article begins on next page)*

![forum acusticum 2023]

# RELATING WAVE-BASED AND GEOMETRIC ACOUSTICS USING A STATIONARY PHASE APPROXIMATION

**Randall Ali**[1]  **Thomas Dietzen**[1]  **Matteo Scerbo**[2]
**Leny Vinceslas**[2]  **Toon van Waterschoot**[1]  **Enzo De Sena**[2]
[1] Department of Electrical Engineering (ESAT-STADIUS), KU Leuven, Belgium
[2] Institute of Sound Recording, University of Surrey, UK

## ABSTRACT

Room acoustic simulation using physically motivated sound propagation models are typically separated into wave-based methods and geometric methods. While each of these methods has been extensively studied, the question on when to transition from a wave-based to a geometric method still remains somewhat unclear. Towards building greater understanding of the links between wave-based and geometric methods, this paper investigates the transition question by using the method of stationary phase. As a starting point, we consider an elementary scenario with a geometrically interpretable analytic solution, namely that of an infinite rigid boundary mirroring a single monopole sound source, and apply the stationary phase approximation (SPA) to the wave-based boundary integral equation (BIE). The results of the analysis demonstrate how net boundary contributions give rise to the geometric interpretation offered by the SPA and provide the conditions when the SPA is asymptotically equal to the analytical solution in this elementary scenario. Although the results are unsurprising and intuitive, the insights gained from this analysis pave the way for investigating relations between wave-based and geometric methods in more complicated room acoustics scenarios.

## 1. INTRODUCTION

Room acoustic simulation using physically motivated sound propagation models is typically separated into two approaches: (i) wave-based methods and (ii) geometric methods, along with hybrids between the two [1–6]. In wave-based methods, the

intention is to solve the wave equation with boundary conditions, which has resulted in several numerical algorithms such as the boundary element method (BEM) [7], finite element method FEM [8], and the finite difference time-domain method (FDTD) [9]. The advantage is that wave-like effects such as diffraction and interference can be accurately modelled, however the computational cost rapidly increases with frequency. Consequently, geometric methods such as ray-tracing [10] and the image method [11] (for non-rigid boundaries) have been proposed where sound propagation is modelled by rays at higher frequencies, easing the computational load, but at the expense of not being able to model wave-like effects.

In this paper, we are interested in gaining a better understanding of the conditions under which wave-based methods cross over into geometric methods. There are several conditions that can already be used to make this distinction such as (a) the Schroeder frequency [12], (b) the frequency beyond which spatial aliasing occurs in wave-based element methods [7], or (c) when the wavelength of sound is much smaller than the dimensions of a room [13]. However, such conditions may not always be sufficient to specify the transition, particularly the Schroeder frequency [2].

In search of additional conditions that can better help us to specify the crossover, we turn to the method of stationary phase [14, 15] to approximate the Kirchoff-Helmholtz integral equation or boundary integral equation (BIE), which is a reformulation of the wave equation with specified boundary conditions. The stationary phase approximation (SPA) is by definition, a high-frequency approximation and hence in using it to approximate the solution to the BIE, we can gain some insight into the transition

from a wave-based to a geometric method. The SPA has in fact been applied to the Rayleigh integral, a particular form of the BIE, but in the context of wave field synthesis [16]. It has also been used to develop BEM algorithms [17] and it is known that the point of stationary phase on a boundary corresponds to the specular reflection point [18, 19], further justifying its usefulness to bridge the gap between wave-based and geometric methods in room acoustic simulation.
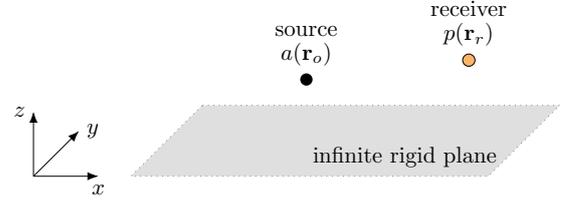
In this work, we consider the elementary scenario of an infinite rigid boundary mirroring a single monopole sound source. While such a scenario is not immediately generalizable to more complicated room acoustics scenarios, we nevertheless proceed to use it because of its geometrically-interpretable analytical solution for which we can compare against. The results that follow demonstrate that the SPA is asymptotically equal to the analytical solution when the distance from the stationary phase point on the boundary to the receiver is much greater than the wavelength. As the SPA is in principle applicable regardless of whether an analytical solution to the BIE exists, the geometric interpretation of the SPA can potentially be an additional tool to address the transition question between wave-based and geometric methods in other room acoustic scenarios.

This paper is organized as follows. In section 2, we review the BIE and the SPA. In section 3, the SPA is applied to the BIE for the infinite rigid boundary scenario. In section 4, we observe how the net boundary contributions are related to the stationary phase point and the impact of the SPA on multiple receivers in space. Section 5 concludes the paper.

## 2. BACKGROUND

We consider the scenario of Fig. 1 with a point source located at $\mathbf{r}_\mathrm{o} = [x_\mathrm{o},\ y_\mathrm{o},\ z_\mathrm{o}]$ and a receiver at $\mathbf{r}_\mathrm{r} = [x_\mathrm{r},\ y_\mathrm{r},\ z_\mathrm{r}]$ above an infinite rigid boundary at $z = 0$. In the frequency domain, the analytical solution for the complex acoustic pressure at the receiver, $p_\mathrm{an}(\mathbf{r}_\mathrm{r})$, is the sum of the acoustic pressure incident from the source and from an equivalent source mirrored on the other side of the boundary [11]:

$$p_\mathrm{an}(\mathbf{r}_\mathrm{r}) = a(\mathbf{r}_\mathrm{o})G(\mathbf{r}_\mathrm{r}|\mathbf{r}_\mathrm{o}) + a(\mathbf{r}_\mathrm{o})G(\mathbf{r}_\mathrm{r}|\mathbf{r}_\mathrm{i}) \qquad (1)$$



**Figure 1**. Source and receiver above an infinite rigid boundary.

where $a(\mathbf{r}_\mathrm{o})$ is the complex pressure amplitude of the source (Pa.m) and $G(\mathbf{v}|\mathbf{u})$ is the free-field Green's function for a monopole source in $\mathbf{u}$, observed in $\mathbf{v}$:

$$G(\mathbf{v}|\mathbf{u}) = \frac{e^{-jk\|\mathbf{v}-\mathbf{u}\|}}{\|\mathbf{v}-\mathbf{u}\|} \qquad (2)$$

where $\|\mathbf{v}-\mathbf{u}\|$ is the Euclidean distance between positions $\mathbf{u}$ and $\mathbf{v}$, $k = \omega/c$ is the wavenumber $(\mathrm{m}^{-1})$, $\omega$ is the angular frequency $(\mathrm{rad\,s}^{-1})$, and $c$ is the speed of sound $(\mathrm{m\,s}^{-1})$. Hence $G(\mathbf{r}_\mathrm{r}|\mathbf{r}_\mathrm{o})$ is the free-field Green's function from the source to the receiver with distance $\|\mathbf{r}_\mathrm{r}-\mathbf{r}_\mathrm{o}\|$, and $G(\mathbf{r}_\mathrm{r}|\mathbf{r}_\mathrm{i})$ is the free-field Green's function from the mirrored (image) source to the receiver with distance $\|\mathbf{r}_\mathrm{r}-\mathbf{r}_\mathrm{i}\|$, where $\mathbf{r}_\mathrm{i} = [x_\mathrm{o},\ y_\mathrm{o},\ -z_\mathrm{o}]$.

### 2.1 Boundary Integral Equation

The BIE is a reformulation of the inhomogeneous wave equation in terms of an integral of acoustic pressure dipoles and velocity monopoles on the boundaries or surfaces enclosing some domain. The acoustic pressure $p(\mathbf{r}_\mathrm{r})$ at a receiver position $\mathbf{r}_\mathrm{r}$ in the domain can be expressed as [7]

$$f(\mathbf{r}_\mathrm{r})p(\mathbf{r}_\mathrm{r}) = 4\pi\, a(\mathbf{r}_\mathrm{o})G(\mathbf{r}_\mathrm{r}|\mathbf{r}_\mathrm{o})$$
$$+ \int_S \left[ p(\mathbf{r}_\mathrm{s})\frac{\partial G(\mathbf{r}_\mathrm{r}|\mathbf{r}_\mathrm{s})}{\partial \mathbf{n}} + j\omega\rho v_\mathrm{n}(\mathbf{r}_\mathrm{s})G(\mathbf{r}_\mathrm{r}|\mathbf{r}_\mathrm{s}) \right] dS \qquad (3)$$

where the first term on the right-hand-side is the acoustic pressure contribution from the source to the receiver (incident pressure). The second term is an integral over the surface, $S$, representing the scattered acoustic pressure, where $\mathbf{r}_\mathrm{s}$ represents the coordinate vector of an arbitrary point on the surface, $p(\mathbf{r}_\mathrm{s})$ is the acoustic pressure on $\mathbf{r}_\mathrm{s}$, $\frac{\partial G(\mathbf{r}_\mathrm{r}|\mathbf{r}_\mathrm{s})}{\partial \mathbf{n}}$ is the normal derivative of the free-field Green's function

where $\mathbf{n}$ is the normal vector on the surface pointing into the domain, $v_{\mathrm{n}}(\mathbf{r}_{\mathrm{s}})$ is the normal velocity on the surface, and $\rho$ is the density of the fluid $(\mathrm{kg\,m^{-3}})$. As (3) is also valid for any receiver position, $\mathbf{r}_{\mathrm{r}}$, the scaling $f(\mathbf{r}_{\mathrm{r}})$ is either $4\pi$ if $\mathbf{r}_{\mathrm{r}}$ is within the domain, $2\pi$ if $\mathbf{r}_{\mathrm{r}}$ is on the surface, or zero otherwise.

For the case of the infinite rigid boundary, $v_{\mathrm{n}}(\mathbf{r}_{\mathrm{s}}) = 0$, hence for a receiver position within the domain, (3) reduces to

$$p(\mathbf{r}_{\mathrm{r}}) = a(\mathbf{r}_{\mathrm{o}})G(\mathbf{r}_{\mathrm{r}}|\mathbf{r}_{\mathrm{o}}) + \frac{1}{4\pi} \int_S p(\mathbf{r}_{\mathrm{s}}) \frac{\partial G(\mathbf{r}_{\mathrm{r}}|\mathbf{r}_{\mathrm{s}})}{\partial \mathbf{n}}\, dS. \tag{4}$$

Furthermore, we can express the surface pressure as the sum of the pressure contributions from the source and its mirror image, so that $p(\mathbf{r}_{\mathrm{s}}) = a(\mathbf{r}_{\mathrm{o}})G(\mathbf{r}_{\mathrm{s}}|\mathbf{r}_{\mathrm{o}}) + a(\mathbf{r}_{\mathrm{o}})G(\mathbf{r}_{\mathrm{s}}|\mathbf{r}_{\mathrm{i}}) = 2a(\mathbf{r}_{\mathrm{o}})\frac{e^{-jkR_{\mathrm{os}}}}{R_{\mathrm{os}}}$, where $R_{\mathrm{os}} = ||\mathbf{r}_{\mathrm{s}} - \mathbf{r}_{\mathrm{o}}||$ is the distance between the source and the surface point. Substitution of this expression and the normal derivative [1] of (2) into (4) then results in

$$p(\mathbf{r}) = a(\mathbf{r}_{\mathrm{o}})G(\mathbf{r}_{\mathrm{r}}|\mathbf{r}_{\mathrm{o}})$$
$$+ \frac{a(\mathbf{r}_{\mathrm{o}})}{2\pi} \int_S \frac{e^{-jk(R_{\mathrm{os}}+R_{\mathrm{sr}})}}{R_{\mathrm{os}}R_{\mathrm{sr}}} \left(\frac{1}{R_{\mathrm{sr}}} + jk\right) \cos\theta_{\mathrm{sr}}\, dS \tag{5}$$

where $R_{\mathrm{sr}} = ||\mathbf{r}_{\mathrm{r}} - \mathbf{r}_{\mathrm{s}}||$ is the distance between the surface point and receiver, and $\cos\theta_{\mathrm{sr}} = \frac{(\mathbf{r}_{\mathrm{r}}-\mathbf{r}_{\mathrm{s}})^T \mathbf{n}}{R_{\mathrm{sr}}}$ is the directional derivative in the direction of the normal vector, hence $\theta_{\mathrm{sr}}$ is the angle between the normal and the vector from the surface to the receiver point. Upon comparison to (1), it is evident that the scattered pressure (integral term) should be equivalent to the contribution from the mirrored source.

## 2.2 Stationary Phase Approximation

The method of stationary phase [14, 15] is a technique for asymptotic evaluation of integrals having the form $\int g(p)\,e^{jk\phi(p)}\,dp$ for $k \to \infty$, to which (5) conforms. For large values of $k$ and when $\nabla\phi(p) \neq 0$ there will be rapid oscillations of the real and imaginary parts of $e^{jk\phi(p)}$ about zero, which consequently result in cancellations and hence decrease the value of the integral [15]. However, if $\nabla\phi(p) = 0$, then

there will be some neighbourhood of points, i.e. the *stationary phase points*, over which $e^{jk\phi(p)}$ does not vary as rapidly, regardless of the value of $k$, and hence do not result in cancellation. In other words, the main contribution to the integral as $k \to \infty$ will depend on $g(p)$ and $\phi(p)$ within the region of stationary phase points where $\nabla\phi(p) = 0$.

With the assumption that $\phi(p)$ has a finite number of stationary phase points in the support of $g(p)$, the stationary phase approximation (SPA) can be computed as follows [14, 15]:

$$\int_{\mathbb{R}^n} g(p)\,e^{jk\phi(p)}\,dp \approx$$
$$\left(\frac{2\pi}{k}\right)^{n/2} \sum_{p_0 \in P} e^{\frac{j\pi}{4}\mathrm{sgn}(\mathbf{H}(p_0))} \frac{g(p_0)\,e^{jk\phi(p_0)}}{\sqrt{|\det(\mathbf{H}(p_0))|}} \tag{6}$$

where $P$ is the set of stationary phase points of $\phi(p)$ for which $\nabla\phi(p) = 0$, $\mathbf{H}(p_0)$ is the Hessian of $\phi(p)$ at $p_0$, $\det(\mathbf{H}(p_0))$ is the determinant of $\mathbf{H}(p_0)$, and $\mathrm{sgn}(\mathbf{H}(p_0))$ is the metric signature of the Hessian, i.e. the number of positive eigenvalues minus the number of negative eigenvalues of the matrix. In the following section we apply the SPA to the BIE of (5).

## 3. STATIONARY PHASE APPROXIMATION FOR AN INFINITE RIGID BOUNDARY

### 3.1 Stationary Phase Point

We will firstly compute the stationary phase point on the infinite rigid boundary. Upon comparison of (5) to (6), we can observe that
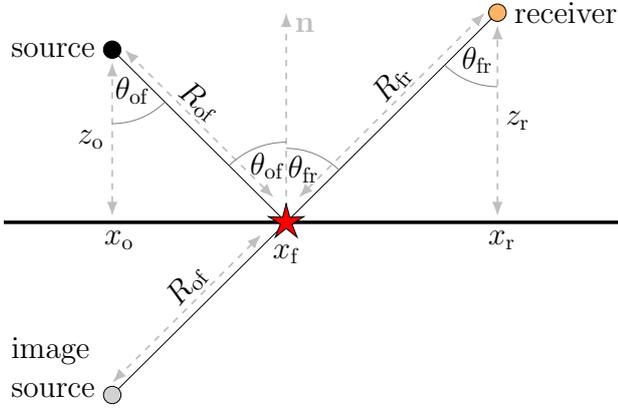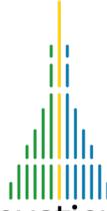
$$\phi(p) = -(R_{\mathrm{os}} + R_{\mathrm{sr}}) \tag{7}$$
$$g(p) = \frac{1}{R_{\mathrm{os}}R_{\mathrm{sr}}} \left(\frac{1}{R_{\mathrm{sr}}} + jk\right) \cos\theta_{\mathrm{sr}} \tag{8}$$

where

$$R_{\mathrm{os}} = R_{\mathrm{os}}(x_{\mathrm{s}}, y_{\mathrm{s}}) = \left((x_{\mathrm{s}} - x_{\mathrm{o}})^2 + (y_{\mathrm{s}} - y_{\mathrm{o}})^2 + z_{\mathrm{o}}^2\right)^{\frac{1}{2}}$$
$$R_{\mathrm{sr}} = R_{\mathrm{sr}}(x_{\mathrm{s}}, y_{\mathrm{s}}) = \left((x_{\mathrm{s}} - x_{\mathrm{r}})^2 + (y_{\mathrm{s}} - y_{\mathrm{r}})^2 + z_{\mathrm{r}}^2\right)^{\frac{1}{2}} \tag{9}$$

with $x_{\mathrm{s}}$ and $y_{\mathrm{s}}$ the $x$-$y$ coordinates on the boundary (recall $z = 0$ on the boundary). The stationary phase

---

[1] We have constrained $\partial G(\mathbf{r}_{\mathrm{r}}|\mathbf{r}_{\mathrm{s}})/\partial \mathbf{n}$ to be positive to ensure a unique solution in the upper half ($z > 0$) of the plane.

**Figure 2**. Geometric interpretation of the stationary phase point (red star) for an infinite rigid boundary depicted in the $x$-$z$ plane.

point is then found by setting $\nabla\phi(p) = \mathbf{0}$:

$$-\frac{\partial\phi(p)}{\partial x_s} = \frac{x_s - x_o}{R_{os}} + \frac{x_s - x_r}{R_{sr}} = 0 \qquad (10)$$

$$-\frac{\partial\phi(p)}{\partial y_s} = \frac{y_s - y_o}{R_{os}} + \frac{y_s - y_r}{R_{sr}} = 0 \qquad (11)$$

which gives the unique solution

$$\begin{aligned} x_s &= x_o \frac{R_{sr}}{R_{os} + R_{sr}} + x_r \frac{R_{os}}{R_{os} + R_{sr}} \triangleq x_f \\ y_s &= y_o \frac{R_{sr}}{R_{os} + R_{sr}} + y_r \frac{R_{os}}{R_{os} + R_{sr}} \triangleq y_f \end{aligned} \qquad (12)$$

and hence the $x$-$y$ coordinates $(x_f, y_f)$ on the boundary defines the stationary phase point.

As a result of setting $\nabla\phi(p) = \mathbf{0}$, the stationary phase point, $(x_f, y_f)$ found in (12) corresponds to the point for which the distance $R_{os} + R_{sr}$ is minimized, which implies that the plane defined by the source, the receiver, and the stationary phase point is orthogonal to the boundary. This brings us to the following geometric interpretation of the stationary phase point as illustrated in Fig. 2, where for ease of depiction and without loss of generality, we assume that the source and receiver lie in the $x$-$z$ plane ($y = 0$). Defining $R_{of} \triangleq R_{os}(x_f, y_f)$, $R_{fr} \triangleq R_{sr}(x_f, y_f)$ and $\theta_{of}, \theta_{fr}$ as shown in Fig. 2, we can deduce from (10) with $x_s = x_f$ that $\sin\theta_{of} = \sin\theta_{fr}$, i.e., the angle of incidence is equal to the angle of reflection and hence the stationary phase point coincides with the point of

specular reflection, which is also the point of intersection between a line from an image source to the receiver and the boundary.

### 3.2 Analysis of the SPA

Continuing with the SPA, we need to compute the determinant of the Hessian of $\phi(x_f, y_f)$, i.e., for $\phi$ evaluated at the stationary phase point. Firstly, the Hessian of $\phi(x_f, y_f)$ is defined as

$$\mathbf{H}(x_f, y_f) = \begin{bmatrix} \frac{\partial^2\phi(x_f,y_f)}{\partial x_f^2} & \frac{\partial^2\phi(x_f,y_f)}{\partial x_f \partial y_f} \\ \frac{\partial^2\phi(x_f,y_f)}{\partial x_f \partial y_f} & \frac{\partial^2\phi(x_f,y_f)}{\partial y_f^2} \end{bmatrix} \qquad (13)$$

where

$$\begin{aligned} \frac{\partial^2\phi(x_f, y_f)}{\partial x_f^2} &= -\frac{1}{R_{of}} + \frac{(x_f - x_o)^2}{R_{of}^3} - \frac{1}{R_{fr}} + \frac{(x_f - x_r)^2}{R_{fr}^3}, \\ \frac{\partial^2\phi(x_f, y_f)}{\partial y_f^2} &= -\frac{1}{R_{of}} + \frac{(y_f - y_o)^2}{R_{of}^3} - \frac{1}{R_{fr}} + \frac{(y_f - y_r)^2}{R_{fr}^3}, \\ \frac{\partial^2\phi(x_f, y_f)}{\partial x_f \partial y_f} &= \frac{(x_f - x_o)(y_f - y_o)}{R_{of}^3} + \frac{(x_f - x_r)(y_f - y_r)}{R_{fr}^3}. \end{aligned} \qquad (14)$$

By substituting (9) (for $(x_s, y_s) = (x_f, y_f)$), we can then obtain the following expression for the determinant of $\mathbf{H}(x_f, y_f)$:

$$\det(\mathbf{H}(x_f, y_f)) =$$
$$\frac{\left(\left((x_f - x_o)(y_f - y_r)\right) - \left((x_f - x_r)(y_f - y_o)\right)\right)^2 \frac{R_{fr}}{R_{of}}}{R_{of}^2 R_{fr}^4}$$
$$+ \frac{z_o^2 \frac{R_{fr}^4}{R_{of}^2} + z_o^2 \frac{R_{fr}^3}{R_{of}} + z_r^2 R_{of} R_{fr} + z_r^2 R_{of}^2}{R_{of}^2 R_{fr}^4} \qquad (15)$$

where using (9) again, it can be shown that

$$z_o^2 \frac{R_{fr}^4}{R_{of}^2} = z_r^2 R_{fr}^2 + (R_{fr}^2 - z_r^2) R_{fr}^2 + \frac{\left(z_o^2 - R_{of}^2\right) R_{fr}^4}{R_{of}^2}$$

$$z_o^2 \frac{R_{fr}^3}{R_{of}} = z_r^2 R_{of} R_{fr} + (R_{fr}^2 - z_r^2) R_{of} R_{fr} + \frac{\left(z_o^2 - R_{of}^2\right) R_{fr}^3}{R_{of}}$$

and hence (15) becomes

$$\det(\mathbf{H}(x_f, y_f)) = \frac{z_r^2 (R_{of} + R_{fr})^2}{R_{of}^2 R_{fr}^4}$$
$$+ \frac{\left(\left((x_f - x_o)(y_f - y_r)\right) - \left((x_f - x_r)(y_f - y_o)\right)\right)^2 \frac{R_{fr}}{R_{of}}}{R_{of}^2 R_{fr}^4}$$
$$+ \frac{(R_{fr} + R_{of}) R_{fr} \left((R_{fr}^2 - z_r^2) - (R_{fr}^2 - \frac{z_o^2 R_{fr}^2}{R_{of}^2})\right)}{R_{of}^2 R_{fr}^4}. \qquad (16)$$

From (12) we can obtain expressions for $(x_\mathrm{f} - x_\mathrm{o})$ and $(y_\mathrm{f} - y_\mathrm{o})$, which upon substituting into (16) then results in the second term of (16) being equal to zero. Furthermore, referring to Fig. 2, we know that $z_\mathrm{r} = R_\mathrm{fr} \cos \theta_\mathrm{fr}$, $z_\mathrm{o} = R_\mathrm{of} \cos \theta_\mathrm{of}$, and $\theta_\mathrm{of} = \theta_\mathrm{fr}$. Hence, $\frac{z_\mathrm{o}^2 R_\mathrm{fr}^2}{R_\mathrm{of}^2} = z_\mathrm{r}^2$, and consequently the third term of (16) is also zero, so that $\det(\mathbf{H}(x_\mathrm{f}, y_\mathrm{f}))$ reduces to

$$\det(\mathbf{H}(x_\mathrm{f}, y_\mathrm{f})) = \frac{\cos^2 \theta_\mathrm{fr}(R_\mathrm{of} + R_\mathrm{fr})^2}{R_\mathrm{of}^2 R_\mathrm{fr}^2} \qquad (17)$$

which is a remarkably simple expression that also describes the Gaussian curvature around the stationary phase point.

In (6), we still need to find $\mathrm{sgn}(\mathbf{H}(x_\mathrm{f}, y_\mathrm{f}))$, which can be deduced by observing the quadratic function $\mathbf{w}^T \mathbf{H}(x_\mathrm{f}, y_\mathrm{f})\mathbf{w}$ for any real non-zero vector, $\mathbf{w}$. Since $\frac{\partial^2 \phi(x_\mathrm{f}, y_\mathrm{f})}{\partial x_\mathrm{f}^2}$ from (14) is negative [2] and $\det(\mathbf{H}(x_\mathrm{f}, y_\mathrm{f}))$ from (16) is positive, then $\mathbf{w}^T \mathbf{H}(x_\mathrm{f}, y_\mathrm{f})\mathbf{w} < 0$, so that $\mathbf{H}(x_\mathrm{f}, y_\mathrm{f})$ is negative definite and hence $\mathrm{sgn}(\mathbf{H}(x_\mathrm{f}, y_\mathrm{f})) = -2$. As we are also integrating over a surface in the BIE, the real coordinate space dimension is $n = 2$ in (6). Finally, substitution of these deductions, along with (7), (8), (17) into (6), and subsequently into (5) results in:

$$p(\mathbf{r}_\mathrm{r}) \approx a(\mathbf{r}_\mathrm{o})G(\mathbf{r}_\mathrm{r}|\mathbf{r}_\mathrm{o}) + a(\mathbf{r}_\mathrm{o})\frac{e^{-jk(R_\mathrm{of}+R_\mathrm{fr})}}{R_\mathrm{of}+R_\mathrm{fr}}\left(1 - \frac{j}{kR_\mathrm{fr}}\right)$$

$$\approx a(\mathbf{r}_\mathrm{o})G(\mathbf{r}_\mathrm{r}|\mathbf{r}_\mathrm{o}) + a(\mathbf{r}_\mathrm{o})G(\mathbf{r}_\mathrm{r}|\mathbf{r}_\mathrm{i})\left(1 - \frac{j}{kR_\mathrm{fr}}\right)$$
$$(18)$$

where $\|\mathbf{r}_\mathrm{r} - \mathbf{r}_\mathrm{i}\| = R_\mathrm{of} + R_\mathrm{fr}$ in $G(\mathbf{r}_\mathrm{r}|\mathbf{r}_\mathrm{i})$ from (1). We can observe that for $kR_\mathrm{fr} \gg 1$, the SPA is asymptotically equal to the analytical solution for the infinite rigid boundary scenario. Recalling that $R_\mathrm{fr}$ is the distance from the stationary phase point to the receiver point and $k = 2\pi/\lambda$, where $\lambda$ is the wavelength, we can interpret $kR_\mathrm{fr} \gg 1$ as a type of far-field condition from the boundary, where $R_\mathrm{fr}$ must be much greater than $\lambda$. Due the geometric interpretation of the stationary phase point as illustrated in Fig. 2 and the derived asymptotically geometric behavior of the SPA in this scenario, the SPA offers a strong geometric interpretation. As the SPA is in principle applicable regardless of whether an analytical solution to

the BIE exists, [3] it suggests that the geometric interpretation of the SPA can be a useful tool to derive additional conditions for transitioning from a wave-based method to a geometric one.

## 4. SIMULATIONS

In order to gain some more intuition about how the net boundary contributions are related to the stationary phase point and the subsequent usefulness of the SPA, we simulate some simple scenarios involving a section of the infinite rigid boundary.

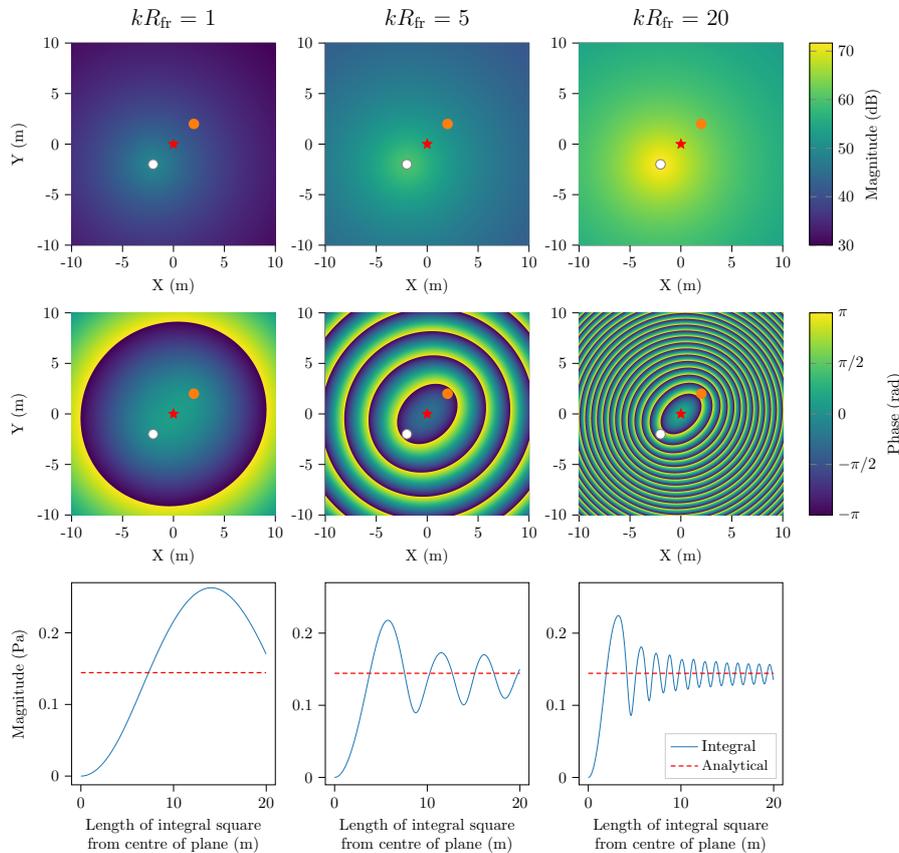### 4.1 Boundary contributions and the stationary phase point

A scenario as depicted in Fig. 1 is considered with a source of complex pressure amplitude $a(\mathbf{r}_\mathrm{o}) = 1j$ Pa.m located at $\mathbf{r}_\mathrm{o} = [-2, -2, 2]$ m and a receiver at $\mathbf{r}_\mathrm{r} = [2, 2, 2]$ m above a 20 m $\times$ 20 m section of the infinite rigid boundary located at $z = 0$. For this scenario, the stationary phase point is $(x_\mathrm{f}, y_\mathrm{f}) = (0, 0)$ m (at the centre of the plane). To understand how the integral from (5) gives rise to the scattered pressure at the receiver, we discretize the boundary, using a spacing of $h = 0.01$ m for the $x$ and $y$ directions, and compute the magnitude and phase of the integrand in the second term from (5).

The top two rows of Fig. 3 show the magnitude (dB re: 20 $\mu Pa$) and phase respectively for $kR_\mathrm{fr} = \{1, 5, 20\}$ over the rigid boundary. The stationary phase point (red star), along with the $(x, y)$ coordinates of the source (white circle) and receiver (orange circle) are also plotted on the boundary.

For all values of $kR_\mathrm{fr}$, the magnitude has a fairly slow and similar variation across the boundary. The maximum magnitude occurs just beneath the source (since this would be the point on the boundary with the shortest distance from the source), which increases for larger values of $kR_\mathrm{fr}$. In the second row of plots, the phase exhibits oscillations which become more rapid with respect to its magnitude as $kR_\mathrm{fr}$ increases. However, there is always an area for which the phase appears relatively constant and this in fact is the region around the stationary phase point.

---

[2] This can be simply shown by making the substitution $\sin \theta_\mathrm{of} = \frac{(x_\mathrm{f} - x_\mathrm{o})}{R_\mathrm{of}}$ and $\sin \theta_\mathrm{fr} = \frac{(x_\mathrm{f} - x_\mathrm{r})}{R_\mathrm{fr}}$ in (14).

[3] If no analytical solution exists, the SPA must however be evaluated numerically.

**10th Convention of the European Acoustics Association**
Turin, Italy • 11th – 15th September 2023 • Politecnico di Torino

EAA

Associazione Italiana di Acustica

**Figure 3**. (Top row) Magnitude (dB re: 20 $\mu Pa$) and (Middle row) Phase contributions of the integrand from (5) over a section of the infinite rigid boundary for $kR_{\text{fr}} = \{1, 5, 20\}$. (Bottom row) Comparing magnitudes from the integral over increasingly large areas with the analytical solution (see text for details).

The effect of increasingly rapid oscillations for larger $kR_{\text{fr}}$ is shown in the plots of the final row of Fig. 1. The blue solid line is the magnitude [4] (Pa) obtained by summing contributions to the integrand in (5) from increasingly larger areas on the boundary starting from the centre of plane (stationary phase point $(0, 0)$) m, and is plotted as a function of the side length of the squares defining these areas. The red dotted line shows the magnitude (Pa) of the second term of the analytical solution from (4).

For $kR_{\text{fr}} = 1$, if we were to extend the 20 m × 20 m boundary to infinity, then summing the contributions over an increasingly large area would show that the magnitude will oscillate around the analytical solution as it does for $kR_{\text{fr}} = 5$ and $kR_{\text{fr}} = 20$.

This demonstrates that the rapid phase variation results in cancellation of the real and imaginary components from the integral of (5), and hence it is only the region around the stationary phase point which is the main contributor to the integral. What is of particular interest though is how large this stationary phase region is with respect to the dimensions of the boundary being considered. In all cases of $kR_{\text{fr}}$, this region is in fact small compared to an infinite boundary. However, if we just observe the 20 m × 20 m boundary, we can see that for an increasing $kR_{\text{fr}}$, the stationary phase region shrinks, so that the main contribution of the integral comes from an increasingly small area on the boundary; an occurrence which was used to develop the scattering algorithm in [17]. It should also be noted that in the limit, this increasingly small area would tend to a sampling of the BIE

---

[4] The phase plots show the same behaviour and are not plotted to be succinct.
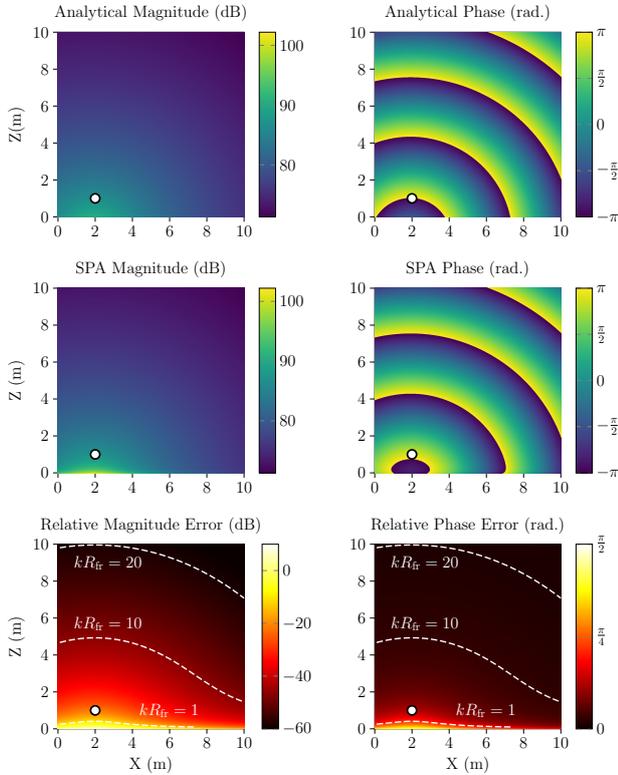
**Figure 4**. Comparison of the analytical magnitude and phase with the SPA for several receiver locations at $k = 2\,\mathrm{m}^{-1}$ (frequency $\approx 109\,\mathrm{Hz}$).

at a single point that is the specular reflection point, which is the basis of geometric methods such as the scattering delay network (SDN) [20].

### 4.2 SPA at multiple receiver locations

A scenario as depicted in Fig. 1 is once again considered with a source of complex pressure amplitude $a(\mathbf{r}_\mathrm{o}) = 1j$ (Pa.m) located at $\mathbf{r}_\mathrm{o} = [2, 3, 1]$ m above an infinite rigid boundary located at $z = 0$. For a range of receiver locations, spaced by $0.01$ m, in the $x$-$z$ plane, with $y_\mathrm{r} = 4$ m, the scattered pressure component using the SPA in (18) as well as that from the analytical solution were computed. The resulting magnitudes are compared in terms of a normalized error, i.e. the absolute value of the difference between the magnitude from the analytical solution and the SPA normalized by the magnitude from the analytical solution (all in Pa). The phases are compared using the absolute value of their difference.

Fig. 4 shows the resulting magnitude and phase from the analytical solution and the SPA, as well as the relative errors between each of these quantities in the $x$-$z$ plane for $k = 2\ \mathrm{m}^{-1}$, a speed of sound, $c = 343\ \mathrm{m\,s}^{-1}$, and hence for a frequency of approximately $109$ Hz. In the first column, the magnitude from the analytical solution and the SPA are plotted in dB re: $20\ \mu Pa$, whereas the relative error is plotted in dB with respect to the magnitude from the analytical solution. In the second column of Fig. 4, the phase from the analytical solution and the SPA are plotted within the range $\{-\pi, \pi\}$, whereas the error is plotted within the range $\{0, \pi/2\}$.

At each receiver location, a different stationary phase point on the boundary had to firstly be computed before the SPA, thus making the value of $kR_\mathrm{fr}$ a function of the receiver location in the $x$-$z$ plane. In Fig. 4 contours (white dotted lines) corresponding to $kR_\mathrm{fr} = \{1, 10, 20\}$ are also plotted on the SPA plots and the error plots, which demonstrate that indeed as $kR_\mathrm{fr} \gg 1$, the SPA converges to the analytical result. We can also expect that as the frequency increases, the SPA will be a good approximation for an increasing larger area in the $x$-$z$ plane with the errors being concentrated near to the boundary. Apart from demonstrating the accuracy of the SPA in this elementary scenario, these results also show the potential of the SPA to obtain additional conditions, such as $kR_\mathrm{fr} \gg 1$, for transitioning from a wave-based to a geometric method.

### 5. CONCLUSION

A stationary phase approximation (SPA) has been applied to the boundary integral equation (BIE) for the scenario of an infinite rigid boundary mirroring a single monopole sound source, as a means to initially investigate the question of when to transition from a wave-based to a geometric method for simulating room acoustics. Relationships between the stationary phase point and the specular reflection point have demonstrated why the SPA can be interpreted as a geometric approximation of solving the wave-based BIE, which is valid when the distance from the stationary phase point to a receiver point is much greater than the wavelength. The results provide some initial insight into the transition question and suggest

that the SPA can be a useful technique for investigating relations between wave-based and geometric methods for simulations in more complicated room acoustics scenarios.

## 6. REFERENCES

[1] M. Vorländer, *Auralization: Fundamentals of Acoustics, Modelling, Simulation, Algorithms and Acoustic Virtual Reality*. Springer, 2008.

[2] M. Vorländer, "Computer simulations in room acoustics: Concepts and uncertainties," *J. Acoust. Soc. Amer.*, vol. 133, no. 3, pp. 1203–1213, 2013.

[3] S. Siltanen, T. Lokki, and L. Savioja, "Rays or waves ? Understanding the strengths and weaknesses of computational room acoustics modeling techniques," in *Proc. of the Int. Symp. Room Acoust., (ISRA 2010)*, pp. 1–6, 2010.

[4] L. Savioja and U. P. Svensson, "Overview of geometrical room acoustic modeling techniques," *J. Acoust. Soc. Amer.*, vol. 138, no. 2, pp. 708–730, 2015.

[5] J. A. Hargreaves, "A comparison between the high-frequency boundary element method and surface-based geometrical acoustics," in *Proc. of Internoise*, p. 251, 2022.

[6] R. Prislan, G. Veble, and D. Svenšek, "Ray-trace modeling of acoustic Green's function based on the semiclassical (eikonal) approximation," *J. Acoust. Soc. Amer.*, vol. 140, no. 4, pp. 2695–2702, 2016.

[7] T. Wu, *Boundary Element Acoustics: Fundamentals and Computer Codes*. WIT, 2000.

[8] R. J. Astley, "Numerical acoustical modeling (finite element modeling)," in *Handbook of Noise and Vibration Control*, ch. 7, pp. 101–115, Wiley, 2007.

[9] B. Hamilton and S. Bilbao, "FDTD methods for 3-D room acoustics simulation with high-order accuracy in space and time," *IEEE/ACM Trans. Audio Speech Lang. Process.*, vol. 25, no. 11, pp. 2112–2124, 2017.

[10] A. Krokstad, S. Strom, and S. Sørsdal, "Calculating the acoustical room response by the use of a ray tracing technique," *J. Sound Vib.*, vol. 8, no. 1, pp. 118–125, 1968.

[11] J. B. Allen and D. A. Berkley, "Image method for efficiently simulating small-room acoustics," *J. Acoust. Soc. Amer.*, vol. 65, no. 4, pp. 943–950, 1979.

[12] M. R. Schroeder, "The "Schroeder frequency" revisited," *J. Acoust. Soc. Amer.*, vol. 99, no. 5, pp. 3240–3241, 1996.

[13] H. Kuttruff, *Room Acoustics, Fifth Edition*. Taylor & Francis, 2009.

[14] V. Guillemin and S. Sternberg, *Geometric Asymptotics*. American Mathematical Society, 1990.

[15] N. Bleistein and R. Handelsman, *Asymptotic Expansions of Integrals*. Dover Publications, 1986.

[16] S. Spors and J. Ahrens, "Analysis and improvement of pre-equalization in 2.5-dimensional wave field synthesis," *in Preprints AES 128th Conv.*, no. 8121, 2010.

[17] O. P. Bruno and C. A. Geuzaine, "An O (1) integration scheme for three-dimensional surface scattering problems," *J. of Comput. Appl. Math*, vol. 204, no. 2, pp. 463–476, 2007.

[18] D. E. Funk and K. L. Williams, "A physically motivated simulation technique for high-frequency forward scattering derived using specular point theory," *J. Acoust. Soc. Amer.*, vol. 91, no. 5, pp. 2606–2614, 1992.

[19] J. Schleicher, M. Tygel, B. Ursin, and N. Bleistein, "The Kirchhoff-Helmholtz integral for anisotropic elastic media," *Wave Motion*, vol. 34, no. 4, pp. 353–364, 2001.

[20] E. De Sena, H. Hacihabiboglu, Z. Cvetkovic, and J. O. Smith, "Efficient synthesis of room acoustics via scattering delay networks," *IEEE Trans. Audio Speech Lang. Process.*, vol. 23, no. 9, pp. 1478–1492, 2015.